Journal of Instrumentation

SISSA

OPEN ACCESS

Monitoring radiation damage in the LHCb Tracker Turicensis

To cite this article: C. Abellan Beteta *et al* 2020 *JINST* **15** P08016

Published by IOP Publishing for Sissa Medialab
Received: *April 1, 2020*
Revised: *June 13, 2020*
Accepted: *June 23, 2020*
Published: *August 25, 2020*

Monitoring radiation damage in the LHCb Tracker Turicensis

The LHCb Silicon Tracker group

C. Abellan Beteta,[a] M. Atzeni,[a] V. Battista,[b] A. Bursche,[i] B. Dey,[j] A. Dosil Suarez,[d] C. Elsasser,[a] A. Fernandez Prieto,[d] J. Fu,[c] E. Graverini,[b] I. Komarov,[b,1] E. Lemos Cid,[d] F. Lionetto,[a] A. Mauri,[g] A. Merli,[c] P.R. Pais,[f,2] E. Perez Trigo,[d] M. del Pilar Peco Regales,[e,3] P. Stefko,[b] O. Steinkamp,[a] B. Storaci,[a] M. Tobin[h] and A. Weiden[a]

[a] *Physik-Institut, Universität Zürich, Zürich, Switzerland*
[b] *Institute of Physics, Ecole Polytechnique Fédérale de Lausanne (EPFL), Lausanne, Switzerland*
[c] *Università degli Studi di Milano, Milano, Italy*
[d] *Instituto Galego de Física de Altas Enerxías (IGFAE), Universidade de Santiago de Compostela, Santiago de Compostela, Spain*
[e] *Max-Planck-Institut für Kernphysik (MPIK), Heidelberg, Germany*
[f] *European Organization for Nuclear Research (CERN), Geneva, Switzerland*
[g] *Nikhef National Institute for Subatomic Physics, Amsterdam, Netherlands*
[h] *Chinese Academy of Sciences, Beijing, China*
[i] *Sezione INFN di Cagliari, Cagliari, Italy*
[j] *Institute of Particle Physics, Central China Normal University, Wuhan, Hubei, China*

E-mail: preema.rennee.pais@cern.ch

Abstract: This paper presents the techniques used to monitor radiation damage in the LHCb Tracker Turicensis during the LHC Runs 1 and 2. Bulk leakage currents in the silicon sensors were monitored continuously, while the full depletion voltages of the sensors were estimated at regular intervals by performing dedicated scans of the charge collection efficiency as a function of the applied bias voltage. Predictions of the expected leakage currents and full depletion voltages are extracted from the simulated radiation profile, the luminosity delivered by the LHC, and the thermal history of the silicon sensors. Good agreement between measurements and predictions is found.

Keywords: Si microstrip and pad detectors; Radiation damage evaluation methods; Radiation damage to detector materials (solid state)

[1] Now at: Deutsches Elektronen-Synchrotron, Hamburg, Germany.
[2] Corresponding author.
[3] Now at: AGH University of Science and Technology, Krakow, Poland.

https://doi.org/10.1088/1748-0221/15/08/P08016

2020 JINST 15 P08016

Contents

2020 JINST 15 P08016

1 Introduction

The LHCb experiment [1] at the LHC was designed to study decays of hadrons containing beauty and charm quarks. Its main goal is to perform precision measurements of *CP* violating observables, and to search for signatures of potential physics beyond the Standard Model in rare decays of such hadrons.

The layout of the LHCb detector during the LHC Runs 1 and 2 is illustrated in figure 1. The detector is a single-arm forward spectrometer that covers polar angles from about 15 mrad to 250 mrad and consists of a vertex locator, a tracking system comprising a single planar tracking station upstream of the spectrometer dipole magnet and three tracking stations downstream of this magnet, two Ring Imaging Cherenkov detectors, a calorimeter system comprising electromagnetic and hadronic calorimeters, and a muon system. In the LHC Run 1, the Silicon Tracker (ST) comprised the tracking station upstream of the dipole magnet, called Tracker Turicensis (TT), and the central part in each of the three tracking stations downstream of the dipole magnet, called Inner Tracker (IT); the outer part of the downstream tracking stations was formed by a straw-tube detector. The tracking system has been dismantled in the context of a substantial detector upgrade for the LHC Run 3. The TT will be replaced by a new silicon strip detector, while the downstream tracker will consist of scintillating fibre planes [2, 3].

The TT employed conventional AC-coupled float-zone p^+-on-n silicon micro-strip sensors that are 500 µm thick and have 512 strips with a pitch of 183 µm and a length of 96 mm. The total silicon volume per sensor is 4512 mm^3. The initial full depletion voltages of the sensors were determined from measurements of the bulk capacitance as a function of applied bias voltage and were found to range between 135 and 275 V.

The TT consisted of one detector box containing four detection layers arranged in two pairs: the first two layers were centered around $z = 232$ cm, and the last two around $z = 262$ cm. An ambient temperature of about 8°C was maintained inside the box. The box was flushed with dry gas (N_2) to avoid condensation on cold surfaces. Silicon sensors within each detection layer were electronically grouped into read-out sectors consisting of one, two, three or four sensors, as illustrated in figure 2. All sensors within a read-out sector were connected in series to a front-end read-out hybrid that carried four 128-channel Beetle chips [4].

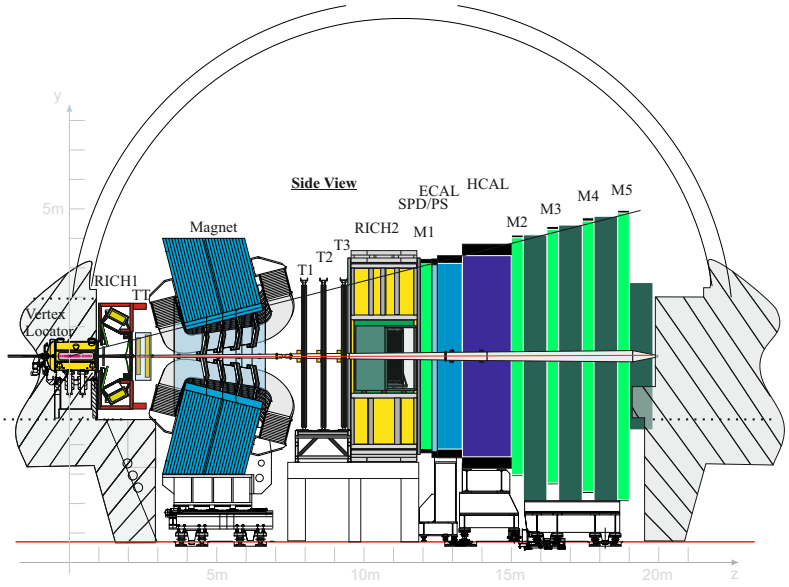

Figure 1. Layout of the LHCb detector: vertex locator (VELO), Ring-Image Cherenkov counters (RICH1 and RICH2), tracking stations upstream (TT) and downstream (T1-T3) of the spectrometer dipole magnet, scintillating pad detector used for trigger purposes (SPD), pre-shower detector (PS) and electromagnetic calorimeter (ECAL), hadronic calorimeter (HCAL), and muon stations (M1-M5). LHCb uses a right-handed cartesian coordinate system with its origin at the nominal interaction point, the z-axis pointing along the LHC beam axis and the y axis pointing upwards.

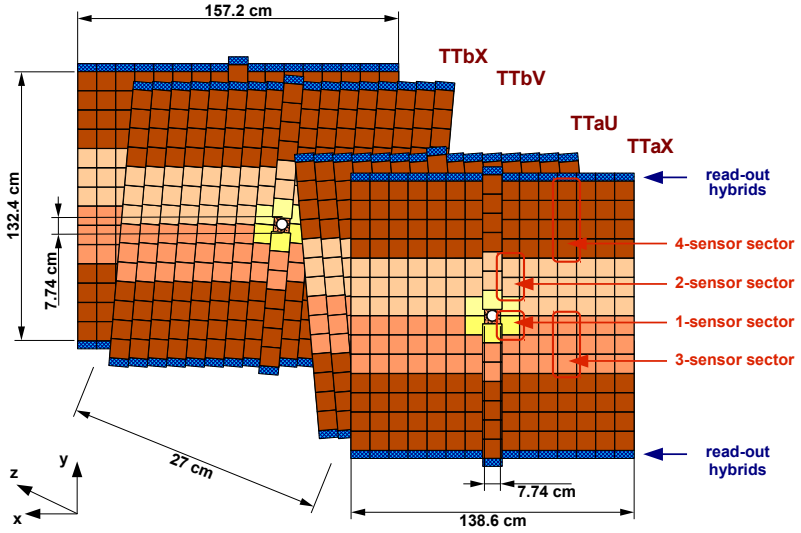

Figure 2. Layout of the TT, with the LHC beam pipe passing through an opening in the centre of the detection layers. The four detection layers are labelled TTaX, TTaU, TTbV and TTbX. The four different types of read-out sectors employed in each of the detection layers are indicated by different shading: read-out sectors close to the beam pipe consist of a single silicon sensor, other read-out sectors consist of two, three or four silicon sensors that are connected together in series.

2020 JINST 15 P08016

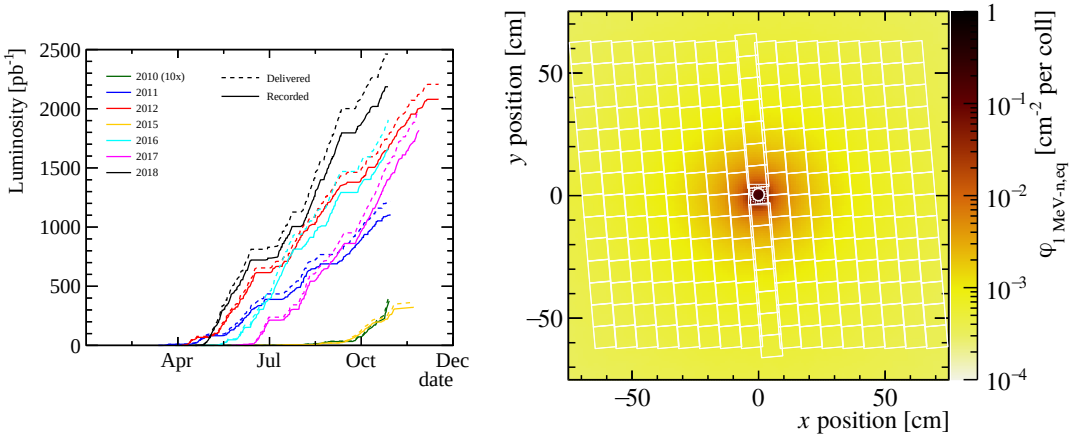

Figure 3. Left: evolution of the integrated luminosity for pp collisions in each year of LHC operation. Right: expected 1-MeV neutron equivalent fluence per proton-proton collision, with the TTaU detector layer overlaid. These results were obtained from a FLUKA simulation of the LHCb detector, assuming a proton-proton collision energy of 14 TeV.

The Beetle front-end read-out chip amplifies and shapes the signals from the read-out strips and samples the signal amplitude every 25 ns, corresponding to the LHC bunch-crossing frequency of 40 MHz. The time offset between the LHC bunch clock and the Beetle sampling time is an adjustable parameter. The output data of the Beetle chips are multiplexed, digitised and transmitted optically to the LHCb TELL1 read-out boards [5]. In the TELL1 boards, algorithms for common-mode subtraction, cluster finding and zero-suppression are executed during normal data taking. It is, however, also possible to store the raw sampled amplitudes from each input channel of the Beetle chip for offline analysis. This non-zero-suppressed read-out mode was employed for the studies discussed in this paper.

LHCb collected an integrated luminosity of about 3 fb^{-1} at proton-proton collision energies of $\sqrt{s}$ =7 and 8 TeV during Run 1 of the LHC (2010–2012), and about 6 fb^{-1} at 13 TeV in Run 2 (2015–2018). The evolution of the integrated luminosity is shown in figure 3 (left) for each year of data taking. Expected particle fluences at collision center-of-mass energies of $\sqrt{s}$ = 7, 8 and 14 TeV have been derived from simulation using FLUKA [6, 7], a general purpose tool for calculations of particle transport and interactions with matter, and a detailed description of the geometry of the LHCb experimental area [8, 9]. Maps of the particle fluence at $\sqrt{s}$ = 7 and 8 TeV are scored with a resolution of [1, 1] cm, while the map at $\sqrt{s}$ = 14 TeV is scored with a resolution of [2.5, 2.5] cm and subsequently interpolated to obtain a map with a resolution of [1, 1] cm. All maps are produced at a z-coordinate corresponding to the location of the TTaU layer. The statistical uncertainty on the expected fluence is modeled as a power-law function of the radial position from the beam pipe, $a_0 \times (r/r_0)^{\alpha}$, where $a_0 = 0.7 \times 10^{-2}$ cm^{-2} , $r_0 = 1$ cm, and $\alpha = 0.918$. The expected 1-MeV neutron equivalent fluence per proton-proton collision at a center-of-mass energy of $\sqrt{s}$ = 14 TeV at the location of one of the detection layers of the TT is shown in figure 3 (right). The highest expected 1-MeV neutron equivalent fluence, in the innermost region of the TT, corresponds to about 10^{13} cm^{-2} per 1 fb^{-1} of integrated luminosity collected at a proton-proton collision energy of $\sqrt{s}$ = 14 TeV. Since particles are primarily produced in the forward direction, the expected

2020 JINST 15 P08016

fluence falls off by almost three orders of magnitude from the innermost to the outermost region of the TT detector.

Two methods were employed to monitor the radiation damage to the silicon sensors and its impact on the detector performance. The first method, discussed in section 2, is based on the continuous measurement of detector leakage currents. These measurements are compared to the expected radiation-induced increase of the bulk leakage current as a function of received fluence at an ambient temperature of 8° C. The second method, discussed in section 3, is based on the analysis of collision data accumulated during dedicated Charge Collection Efficiency (CCE) scans. These CCE scans were performed at regular intervals and allow an estimation of the full depletion voltage of the sensors. The results of these measurements are compared to predictions derived from the Hamburg model [10], which parametrises the evolution of the effective doping concentration of the silicon bulk as a function of received fluence and temperature. Section 4 presents a summary of the different studies and discusses the expected evolution of the TT performance in terms of radiation damage.

2 Leakage current measurements

Bias voltage for the TT was supplied by a commercial high-voltage (HV) system[1] with 152 channels supplying up to 500 V at a maximum current of 10 mA per HV channel. The innermost six silicon sensors in each detection layer, which received the highest fluence and therefore experienced the largest increase in leakage current, were connected to individual HV channels. In the outer regions of the detection layers, groups of two, three, four, nine or twelve silicon sensors were connected to a common HV channel. The current drawn by each HV channel was monitored with a resolution of 1.0 μA, and a maximum interval of 120 minutes allowed between consecutive readings. For the purpose of this analysis, the leakage current, I_{leak}, for a given HV channel is determined for each LHC fill as the maximum current observed in that fill.[2] Measurements from fills with special detector configurations (*e.g.* higher or lower bias voltage) are discarded in the leakage current measurements. The leakage current has a temperature dependent behaviour given by

$$\frac{I_{\text{leak}}(T_1)}{I_{\text{leak}}(T_2)} = \left(\frac{T_1}{T_2}\right)^2 \exp\left[\frac{E_{\text{eff}}}{2k_B}\left(\frac{1}{T_2} - \frac{1}{T_1}\right)\right], \tag{2.1}$$

where $T_{1,2}$ are different temperatures, k_B is the Boltzmann constant and $E_{\text{eff}} = 1.21\,\text{eV}$ is the effective energy for the temperature dependence of the bulk current in irradiated silicon sensors, shown to be temperature-independent in ref. [11]. All measured currents are normalised to a nominal temperature of 8°C, using measurements of the ambient temperature inside the detector box and the well-known temperature dependence of the bulk leakage current in silicon [12].

The normalized leakage currents, scaled to 8°C and per silicon volume, are shown as a function of integrated delivered luminosity and time in figure 4 for the innermost sensors in the second and third detection layers, indicated as U and V layers, respectively.

The change ΔI_{leak} in the leakage current is expected to be linear as a function of the fluence, Φ, that the sensor has been exposed to, for a range between 10^{11} and 10^{15} 1-MeV n / cm^2 [10]. So

[1] CAEN SY1527 crates with A1511B modules, by CAEN S.p.A., Viareggio, Italy.

[2] A typical LHC fill is several hours in duration.

2020 JINST 15 P08016

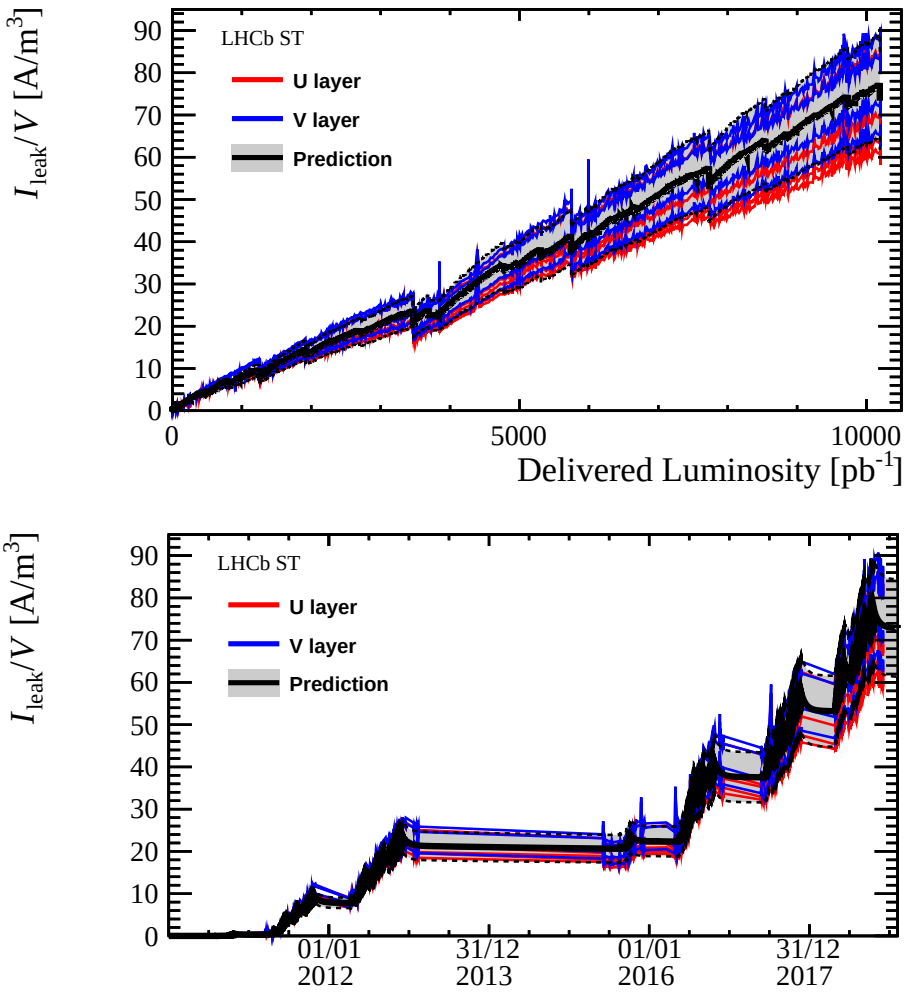

Figure 4. Evolution of the leakage current for the different HV channels connected to one-sensor read-out sectors in TT as a function of (a) the delivered integrated luminosity measured and (b) time. The red curves show channels in the detector layer TTaU, the blue one in TTbV. The predicted evolution is shown in black while the grey band shows its uncertainty, computed from the uncertainty on the model parameters, on the FLUKA simulation and on the temperature measurements. The uncertainty does not account for the range of fluence expected across the sectors shown.

Table 1. Parameters for the leakage current predictions.

Parameter	Value
$\alpha_{I,0}$	$(6.67 \pm 0.09)\times10^{-17}$ A/cm
$\alpha_{I,1}$	$(7.23 \pm 0.06)\times10^{-17}$ A/cm
$\alpha_{I,2}$	$(3.08 \pm 0.07)\times10^{-18}$ A/cm
k_0	$(4.2 \pm 0.5)\times10^{13}$ s^{-1}
E_a	(1.11 ± 0.05) eV

2020 JINST 15 P08016

ΔI_{leak} can be described as

$$\Delta I_{\text{leak}} = \alpha \cdot \Phi \cdot V, \tag{2.2}$$

where α is the current-related damage rate and V the silicon volume. The coefficient α shows a behaviour dependent on temperature, T_a, and on time, t, as the irradiation occurs alternating with annealing, *i.e.* periods without collisions [13]. Short term annealing (on the order of a few days to a month) is described by the sum of a constant and exponential terms, where the first term describes the effects of stable damage. An additional logarithmic term is used to describe annealing effects for time periods longer than a year [14],

$$\alpha(t, T_a) = \alpha_{I,0} + \alpha_{I,1} \exp\Big(- t/\tau_I(T_a)\Big) + \alpha_2 \log\Big(t/t_0\Big). \tag{2.3}$$

The temperature dependence of the time constant τ_I in eq. (2.3) can be described by the Arrhenius relation [15],

$$\tau_I(T_a) = \left[k_{I,0} \exp\left(- \frac{E_{a,I}}{k_B T_a}\right)\right]^{-1}, \tag{2.4}$$

where $k_{I,0}$ is the frequency factor and $E_{a,I}$ the activation energy of the process. The values of these parameters are listed in table 1.

Figure 4 also shows the predicted evolution of I_{leak} based on this formalism using the actual running conditions in LHCb (*i.e.* instantaneous luminosity, duration of the fills, ambient temperature) and the 1-MeV neutron equivalent fluence computed for a given sector by integrating the simulated FLUKA radiation map over the sensor area.

The predictions are in good agreement with the evolution of the leakage currents in data. Significant decreases in the currents are observed, as expected, in the data during periods with no irradiation, *i.e.* in the long shutdown, LS1, of the LHC in 2013 and 2014, extended stops of the accelerator during the winter season and short technical stops throughout the year (one week about every three months).

3 Depletion voltage measurements

Non-ionizing energy loss (NIEL) damage in the silicon bulk leads to a change in the effective doping concentration, n_{eff}, of the bulk and therefore to a change in the full depletion voltage V_{depl} since the two quantities are proportional to each other according to the relation

$$V_{\text{depl}} = \frac{q}{2\varepsilon\varepsilon_0} n_{\text{eff}} D^2, \tag{3.1}$$

where q is the electron charge, $\varepsilon\varepsilon_0$ the effective permittivity of silicon and D the full thickness of the sensor.

As mentioned in section 1, the initial full depletion voltage of all silicon sensors was determined in $C-V$ scans at the foundry and during the construction of the detector. For a subset of the installed detectors, the evolution of V_{depl} during operation has then been measured from scans of the charge-collection efficiency as a function of the applied bias voltage (CCE scans). Such CCE scans require particles from LHC collisions to be recorded using special data taking settings. They are performed about two to four times a year, in particular once at the beginning of LHC operation in spring

2020 JINST 15 P08016

Table 2. Summary of CCE scans dates and corresponding integrated delivered luminosity.

Date	Integrated Luminosity [fb^{-1}]		
	7 TeV	8 TeV	13 TeV
2011-07-14	0.48	—	—
2011-09-07	0.81	—	—
2011-10-25	1.24	—	—
2012-04-05	1.26	0.01	—
2012-07-02	1.26	0.66	—
2012-09-28	1.26	1.46	—
2015-06-03	1.26	2.21	0.00
2015-10-20	1.26	2.21	0.23
2016-04-23	1.26	2.21	0.37
2016-08-04	1.26	2.21	1.34
2017-06-05	1.26	2.21	2.28
2017-07-12	1.26	2.21	2.51
2017-09-12	1.26	2.21	3.21
2017-10-27	1.26	2.21	3.81
2017-11-21	1.26	2.21	4.16
2018-04-17	1.26	2.21	4.26
2018-06-26	1.26	2.21	5.07
2018-09-23	1.26	2.21	6.26

and once at the end of operation before Christmas. Table 2 summarises the CCE scans performed between 2011 and 2018. Few CCE scans have been removed from the analysis due to operational inconsistencies, and are not listed in the table.

While in the nominal data taking configuration the applied bias voltage V_{bias} was 300 V for all TT read-out sectors, during a CCE scan the V_{bias} of one detection layer (TTaU) is scanned in a 60 V to 400 V range. The other detection layers are operated at the nominal bias voltage. The data from these layers and from the other detectors of the LHCb tracking system are used to reconstruct the trajectories of charged particles produced in the proton-proton collisions.

Each CCE scan consists of 66 different data taking configurations. For each of the 11 bias voltage steps, 6 sampling time steps are performed. As the drift velocity of charge carriers and therefore the signal collection time depends on the applied bias voltage, in fact, a scan of the signal sampling time of the Beetle front-end ASIC is performed for each bias voltage setting in the range $\delta t = -9.38, -4.69, 0.00, 4.69, 9.38, 14.06$ ns with respect to the nominal sampling time. A minimum number of 500000 events are recorded for each calibration step, which roughly corresponds to a total of 2–3 hours of data taking depending on the beam configuration at the time of the CCE scan. These scans are mainly taken during the beam commissioning phase, when only a small number of proton bunches circulate in the accelerator, in order to minimize the loss of useful data for physics analysis.

Tracks reconstructed by the rest of the LHCb tracking system, including the TT layers operating in nominal conditions, are used to interpolate the hit position in the scanned layer. Track quality requirements are applied to remove tracks with poor track fit quality or originating from random

2020 JINST 15 P08016

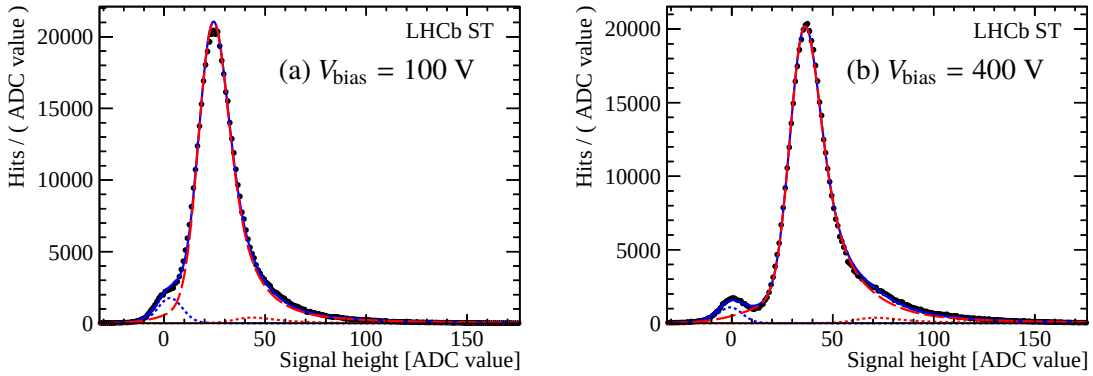

Figure 5. Signal height distribution for hits associated to tracks in the TT for two different bias voltage values. The fitted distribution is described in the text.

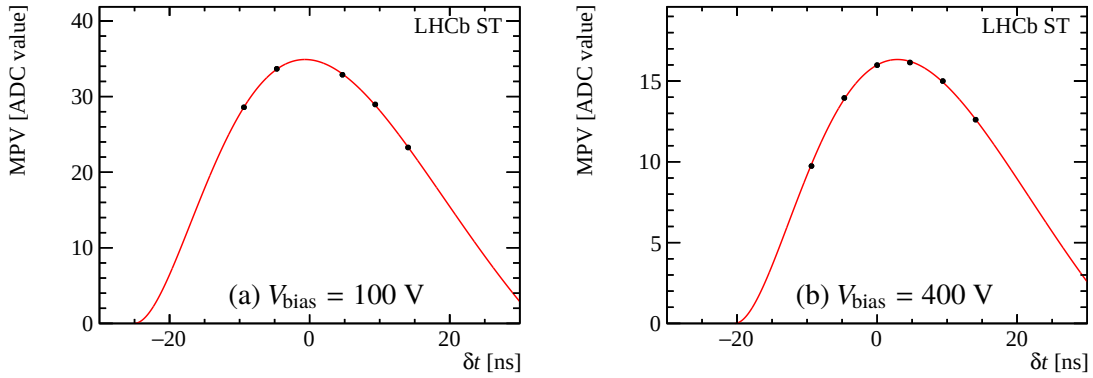

Figure 6. Pulse shapes recorded in the TT for two different bias voltage values. The fitted function is shown in eq. (3.2).

combinations of track segments from different parts of the tracking system. The pedestal-subtracted ADC values of the three read-out strips closest to this interpolated hit position are then summed to give an estimate of the collected charge. As an example, figure 5 shows the signal height distribution in a TT read-out sector for $V_{\text{bias}} = 100$ V and 400 V with $\delta t = 0.00$ ns. The incomplete depletion of the silicon bulk at $V_{\text{bias}} = 100$ V induces the clearly visible decrease in signal amplitude.

The most probable value (MPV) of the collected charge is extracted from a fit of this distribution, using a model consisting of the sum of two Gaussians to describe the residual contribution of noise hits due to wrong track extrapolations (blue line), convolved with the sum of two Landau distributions to describe the contribution from signal hits (red line). The second Landau distribution describes a signal component due to photon conversions in the beam pipe and detector material upstream of the TT, creating e^+e^- pairs that will cross the TT at the same position and deposit twice as much charge as a single track. The MPV and the width of this second Landau distribution are fixed to twice the corresponding values of the first Landau.

The MPVs extracted for different sampling times δt at a given bias voltage are then fit with the empirical function

$$f(\delta t|\tau, t_0, A) = A \cdot \exp\left(-\frac{\delta t - t_0}{\tau}\right) \cdot \left[\frac{1}{2}\left(\frac{\delta t - t_0}{\tau}\right)^2 - \frac{1}{6}\left(\frac{\delta t - t_0}{\tau}\right)^3\right] \tag{3.2}$$

2020 JINST 15 P08016

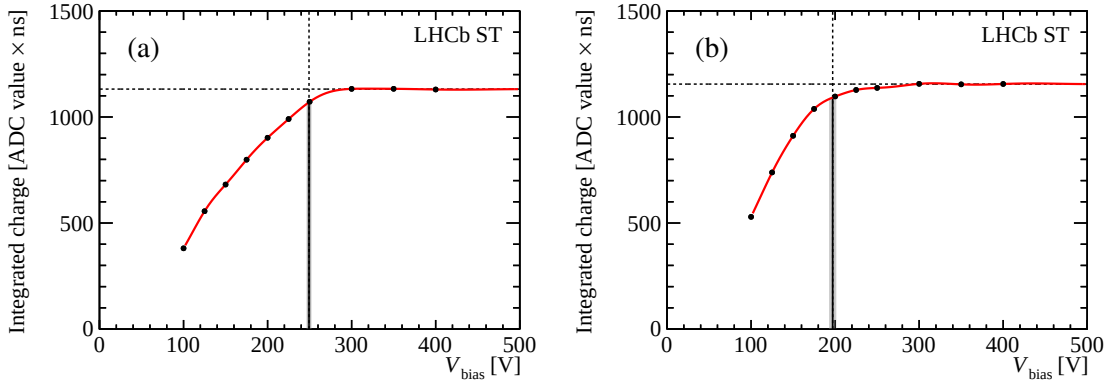

Figure 7. Integrated charge as a function of the applied bias voltage for a central TT read-out sector measured in the CCE scans from (a) April 2012 and (b) September 2017. The decrease of V_{depl} is clearly visible.

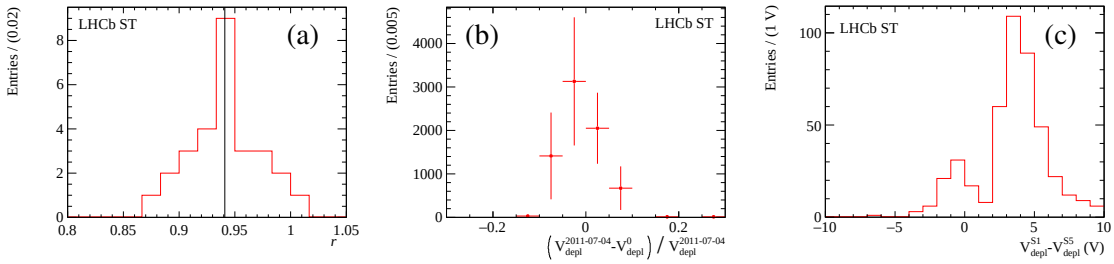

Figure 8. Distributions for all analysed read-out sectors of (a) the ratio r defined in eq. 3.3; (b) the relative difference between V_{depl} and $V^{2011\text{-}07\text{-}04}_{\text{depl}}$ as discussed in the main text; (c) the differences in V_{depl} obtained from a fifth-order spline and from a linear interpolation. The solid black line in (a) highlights the value of the average $\bar{r}$.

describing the semi-Gaussian signal shape output by the pulse shaping circuit employed in the Beetle chip, which is composed of a differentiator (CR) followed by an integrator (RC) [16, 17]. The shaping time τ, time offset t_0 and amplitude A are free parameters of the fit. As an example, figure 6 shows the results of these fits for one of the innermost sensors and for $V_{\text{bias}} = 100$ V and 400 V. The integral of the fitted function between its two zeroes t_0 and $t_0 + 3\tau$ is taken as a measure of the collected charge at the given bias voltage.

This quantity, referred to as "integrated charge", is shown as a function of V_{bias} in figure 7. The three highest V_{bias} data points are fit with a constant to determine the plateau value. The data points are interpolated with a fifth-order spline [18] S and the depletion voltage is determined as the bias voltage at which $S(V_{\text{bias}})$ reaches the fraction $\bar{r} = 94\%$ of its value in the plateau. The value $\bar{r} = 94\%$ was chosen based on an analysis of the earliest CCE scan, taken on 2011-07-14. First, the ratio

$$r = S\left(V^{2011\text{-}07\text{-}14}_{\text{depl}}\right) / S\,(\text{plateau}) \tag{3.3}$$

was calculated for each analysed read-out sector, where the true depletion voltage at the time of the CCE scan, $V^{2011\text{-}07\text{-}04}_{\text{depl}}$, was estimated from the full depletion voltage of the sensor as measured in $C - V$ scans during the construction of the detector, corrected for the expected change in full

2020 JINST 15 P08016

Table 3. Parameters for the depletion voltage simulation by the Hamburg model [10].

Parameter	Value
$n_{c,0}$	$(3.28 \pm 0.26) \times 10^{-10}\,\mathrm{cm}^{-3}$
c	$2.29 \times 10^{-13}\,\mathrm{cm}^{2}$
g_c	$(1.60 \pm 0.04) \times 10^{-2}\ \mathrm{cm}^{-1}$
g_a	$(1.40 \pm 0.14) \times 10^{-2}\ \mathrm{cm}^{-1}$
g_r	$(5.70 \pm 0.09) \times 10^{-2}\ \mathrm{cm}^{-1}$
$k_{a,0}$	$(2.4 \pm 1.0) \times 10^{15}\ \mathrm{s}^{-1}$
$k_{r,0}$	$(1.5 \pm 1.1) \times 10^{15}\ \mathrm{s}^{-1}$
E_{aa}	(1.09 ± 0.03) eV
E_{ar}	(1.31 ± 0.03) eV

depletion voltage according to the Hamburg model and the integrated fluence received at the time of the CCE scan. The distribution of r for all analysed read-out sectors is shown in figure 8(a). The values of r obtained for the different read-out sectors were then averaged to determine $\bar{r}$.

The systematic uncertainty on V_{depl} due to the choice of $\bar{r}$ was estimated by applying the full method to the first CCE scan and comparing the values of V_{depl} extracted from the spline fits with $\bar{r} = 94\%$ to the values $V_{\mathrm{depl}}^{\text{2011-07-04}}$ extracted from the initial $C-V$ scans and the Hamburg model. The residual distribution of V_{depl} and $V_{\mathrm{depl}}^{\text{2011-07-04}}$ is shown in figure 8(b); the spread of this distribution is taken as systematic uncertainty.

A second source of systematic uncertainty is the choice of a fifth-order spline to interpolate the measurements. To estimate this uncertainty, the entire procedure was repeated using a simple linear interpolation between consecutive measurements instead of the spline fit. The distribution of the differences in V_{depl} obtained using the two types of interpolation are shown in figure 8(c) for all analysed read-out sectors; the spread of this distribution is taken as systematic uncertainty. These two uncertainties are summed in quadrature.

The change Δn_{eff} in the effective doping concentration is described in the Hamburg model by three different mechanisms, described in detail in refs. [10, 19–21]:

1. a contribution associated to the effective (incomplete) removal of donor atoms and the addition of stable acceptor atoms due to radiation-induced changes in the band structure of the silicon crystal. This contribution, referred to as "stable damage", is described by

$$\Delta n_c(\Phi_{1\ \mathrm{MeV\text{-}n,eq}}) = n_{c,0}\left[1 - \exp(-c\,\Phi_{1\ \mathrm{MeV\text{-}n,eq}})\right] + g_c\,\Phi_{1\ \mathrm{MeV\text{-}n,eq}}; \tag{3.4}$$

2. a temperature-dependent contribution due to the annealing of the induced defects, which can be described by

$$\Delta n_a(\Phi_{1\ \mathrm{MeV\text{-}n,eq}}, t, T_a) = \Phi_{1\ \mathrm{MeV\text{-}n,eq}}\, g_a \exp\left(-\frac{t}{\tau_a(T_a)}\right); \tag{3.5}$$

2020 JINST 15 P08016

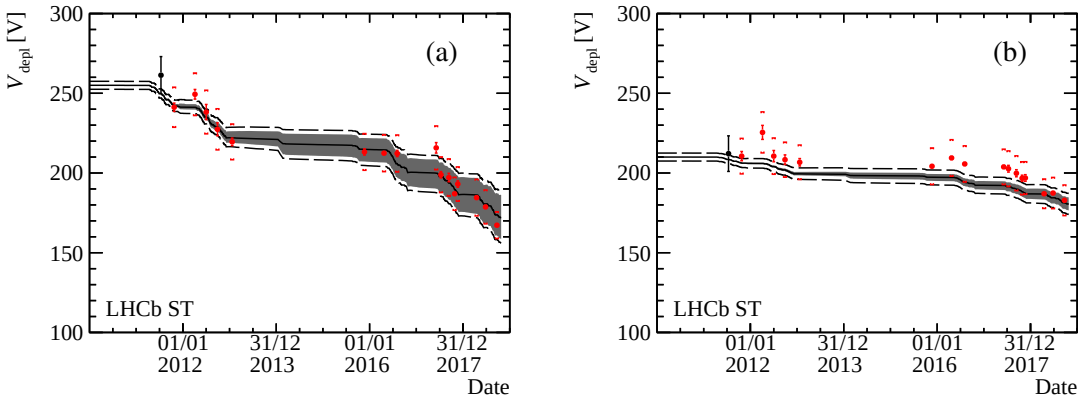

Figure 9. Measured effective depletion voltage (red points) in the area of two TT sensors: one just above the beam pipe (a) and one further away (b), whose positions are indicated in figure 11(a). The black point and error bars correspond to the CCE scan used to calibrate the ratio r. The statistical contribution to the total uncertainty is indicated by the solid error bars. The predicted evolution of the depletion voltage, based on the initial depletion voltage measured after sensor production, the running conditions and the Hamburg model, is shown as a solid black line. The grey bands show the uncertainty on the predicted evolution of V_{depl}, while the black dashed lines account for the ±2.5 V uncertainty on the measurement of the initial depletion voltage V^0_{depl} in $C - V$ scans.

3. a contribution due to the combination of individual defects in the silicon lattice, leading to stable defects ("reverse annealing"), described by

$$\Delta n_r(\Phi_{1\text{ MeV-n,eq}}, t, T_a) = \Phi_{1\text{ MeV-n,eq}}\, g_r \left(1 - \frac{1}{1 + t/\tau_r(T_a)}\right). \tag{3.6}$$

The sum of the three contributions describes the total change of n_{eff}:

$$\Delta n_{\text{eff}} = \Delta n_c + \Delta n_a + \Delta n_r. \tag{3.7}$$

The values of the model parameters are listed in table 3. Their values were measured in dedicated irradiation campaigns and can be found in Reference [10]. The parameters τ_a and τ_r have a temperature dependence described by the Arrhenius relation, *cf.* eq. 2.4, with parameters E_{aa} and $k_{a,0}$ and E_{ar} and $k_{r,0}$, respectively, and the ambient temperature T_a is taken from sensors placed inside the detector boxes.

Figure 9 shows the measured depletion voltages for a one-sensor and for a two-sensors TT read-out sectors, highlighted in figure 11(a), and their predicted evolution based on the Hamburg model described above. This calculation uses the fluence estimated from the FLUKA simulations,[3] the actual running conditions and the temperature measurements in the detector boxes.

For the read-out sectors closest to the LHC beam pipe, dedicated measurements only including tracks traversing the sensors within 75 mm from the beam axis are performed. Figure 10 shows the measured values of V_{depl} of the different TT read-out sectors in the different CCE scans as a function of the 1-MeV-neutron equivalent fluence estimated from the FLUKA simulations and the

[3]Fluence is calculated by integrating the radiation map over the sensor area.

2020 JINST 15 P08016

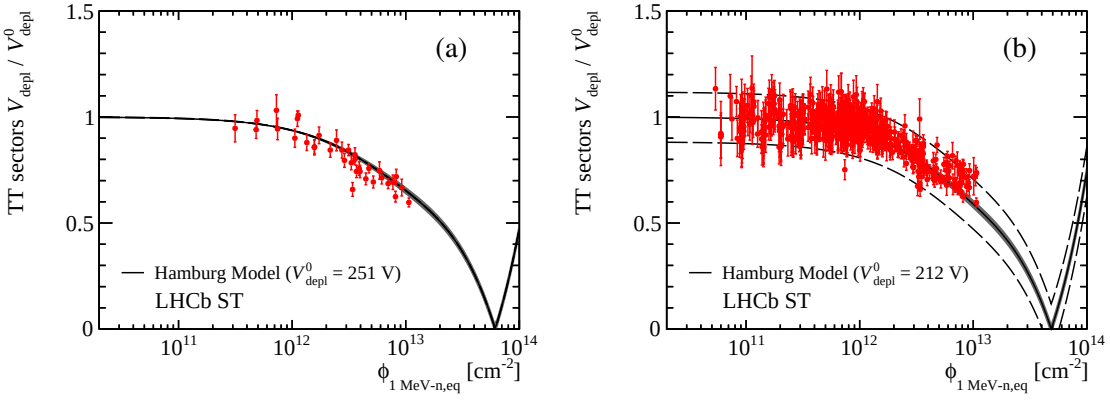

Figure 10. Measured evolution of V_{depl} as a function of the 1-MeV neutron equivalent fluence obtained from the running conditions and FLUKA for a TT sector in the area close to the beam pipe (a) and for all of the read-out sectors in the TT (b). The innermost sectors are subdivided in regions separating tracks traversing the detector at a distance larger or smaller than 75 mm from the beam axis. The error bars of the data points display the sum of the statistical and systematic uncertainty. The solid black curve shows the predictions based on the stable damage part of the Hamburg model, the grey shaded region its uncertainty due to the parameter uncertainty of the model. The initial depletion voltage V^0_{depl} for the Hamburg model prediction in (b) is averaged among all sectors, and the dashed black lines show the standard deviation of the distribution of the initial V^0_{depl} values.

integrated luminosity collected in LHCb. It also shows the expected evolution of V_{depl} based on the stable damage contribution n_c.

Figure 11(c) shows the absolute change of V_{depl} in the innermost part of the detector between July 2011 and September 2018.

Good agreement between the measurements and the predicted evolution of V_{depl} is observed, with no type inversion seen in the silicon sensors of the TT at the end of the LHC Run 2.

4 Conclusion

The evolution of the radiation damage in the LHCb Tracker Turicensis has been monitored using measurements of leakage currents and effective depletion voltages. The latter were performed with data collected in dedicated charge collection efficiency scans. The obtained results show good agreement with predictions based on phenomenological models. At the end of 2018, the innermost sensors, which experience the highest fluence, had not yet reached the point of type inversion, and no modifications to the operation procedure of the detector were performed in its last year of operation. The detector has been dismantled and will be replaced as part of the LHCb upgrade [2, 3] during the long shutdown LS2 of the LHC.

Acknowledgments

E.G. gratefully acknowledges support by the Forschungskredit of the University of Zurich, grant no. FK-17-108. The work of M.A. is supported by the Swiss National Science Foundation (SNF) under contract BSSGI0_155990.

2020 JINST 15 P08016

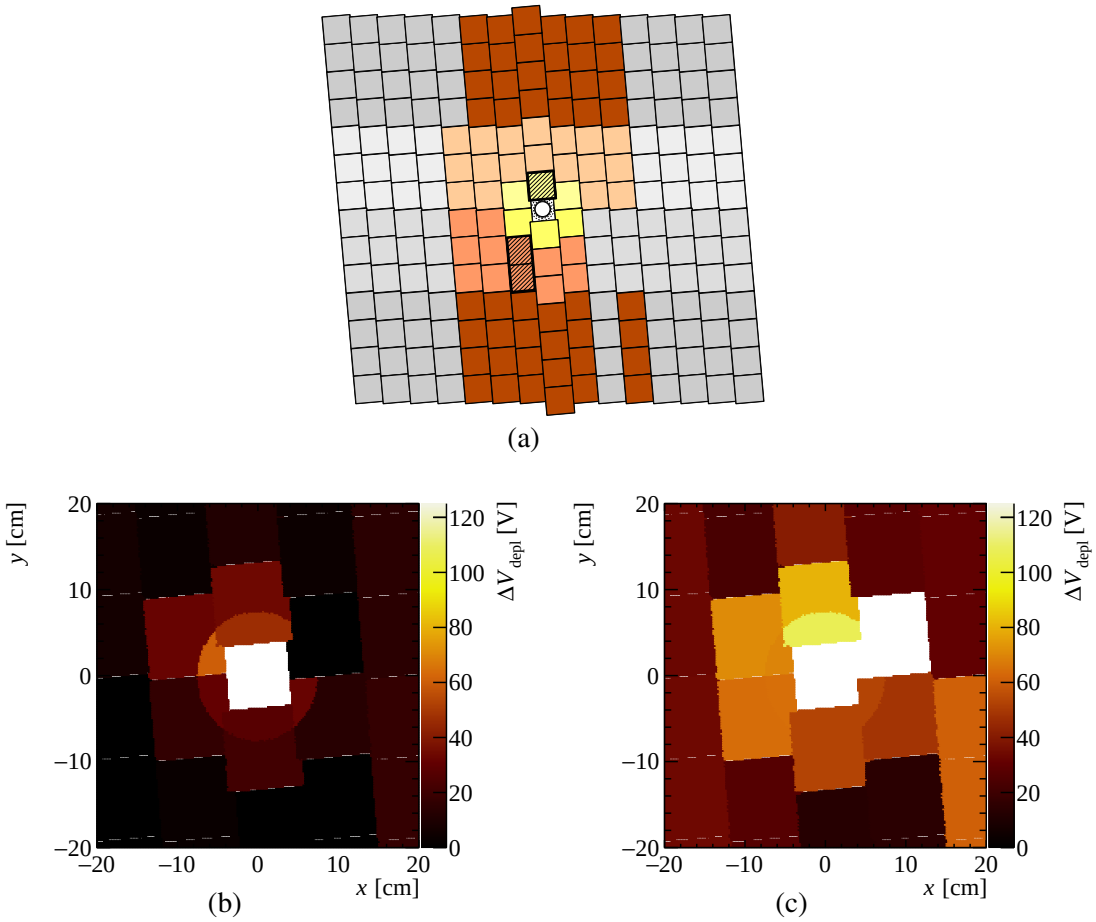

Figure 11. Sketch highlighting the TT sectors analysed during the various CCE scans (a). The greyed out sectors were excluded due to poor statistics. The two sectors highlighted with dashes, just above the beam pipe and below the beam pipe on the left hand side, are those which evolution is shown in figure 9(a) and figure 9(b), respectively. Absolute change in V_{depl} in the innermost region of TT in January 2013 and September 2018 is shown in (b) and (c) respectively. The white sector in (c) became inoperative in August 2017 due to an HV connector issue.

References

[1] LHCb collaboration, *The LHCb detector at the LHC*, 2008 *JINST* **3** S08005.

[2] LHCb collaboration, *Framework TDR for the LHCb upgrade: technical design report*, CERN-LHCC-2012-007 (2012) [LHCb-TDR-12].

[3] LHCb collaboration, *LHCb Tracker Upgrade technical design report*, CERN-LHCC-2014-001 (2014) [LHCB-TDR-015].

[4] M. Agari et al., *Beetle: A radiation hard readout chip for the LHCb experiment*, *Nucl. Instrum. Meth. A* **518** (2004) 468.

[5] G. Haefeli et al., *The LHCb DAQ interface board TELL1*, *Nucl. Instrum. Meth. A* **560** (2006) 494.

[6] A. Ferrari, P.R. Sala, A. Fasso and J. Ranft, *FLUKA: a multi-particle transport code (Program version 2005)*, CERN-2005-010 (2005) [SLAC-R-773].

2020 JINST 15 P08016

[7] G. Battistoni et al., *The FLUKA code: description and benchmarking*, *AIP Conf. Proc.* **896** (2007) 31.

[8] M. Karacson, *Evaluation of the radiation environment of the LHCb experiment*, Ph.D. Thesis, Technische Universität Wien, Vienna, Austria (2016) [CERN-THESIS-2016-246].

[9] G. Corti and L.I. Shekhtman, *Estimation of induced radioactivity in LHCb to determine the reference waste zoning of the experiment*, LHCb-2007-097 (2007) [CERN-LHCb-2007-097].

[10] M. Moll, *Radiation damage in silicon particle detectors: microscopic defects and macroscopic properties*, Ph.D. thesis, Hamburg University, Hamburg, Germany (1999).

[11] A. Chilingarov, *Temperature dependence of the current generated in Si bulk*, 2013 *JINST* **8** P10003.

[12] M. Sze and K. Ng, *Physics of semiconductor devices*, 3rd edition, Wiley, U.S.A. (2006).

[13] M. Moll, E. Fretwurst, G. Lindström and M. Kuhnke, *Relation between microscopic defects and macroscopic changes in silicon detector properties after hadron irradiation*, *Nucl. Instrum. Meth. B* **186** (2002) 100.

[14] CERN-ROSE/RD48 collaboration, *Leakage current of hadron irradiated silicon detectors-material dependence*, *Nucl. Instrum. Meth. A* **426** (1999) 87.

[15] S. Arrhenius, *Über die Dissociationswärme und den Einfluss der Temperatur auf den Dissociationsgrad der Elektrolyte*, *Z. Physik. Chem.* **4** (1889) 96.

[16] S. Lochner, *Development, optimisation and characterisation of a radiation hard mixed-signal readout chip for LHCb*, Ph.D. thesis, Heidelberg University, Heidelberg, Germany (2006).

[17] C. Elsasser, *The rare decays $B^0_{(s)} \to \mu^+\mu^-$ and Z boson production at LHCb and radiation damage in its silicon tracker*, Ph.D. thesis, (2014).

[18] J. Ferguson, *Multivariable curve interpolation*, *J. ACM* **11** (1964) 221.

[19] R. Wunstorf, *A systematic investigation of the radiation hardness of silicon detectors for high-energy physics experiments*, Ph.D. thesis, Hamburg University, Hamburg, Germany (1992).

[20] RD2 collaboration, *Reverse annealing of the effective impurity concentration and long term operational scenario for silicon detectors in future collider experiments*, *Nucl. Instrum. Meth. A* **342** (1994) 119.

[21] H. Feick, *Radiation tolerance of silicon particle detectors for high-energy physics experiments*, PhD thesis, Hamburg University, Hamburg, Germany (1997).

2020 JINST 15 P08016